SANDIA REPORT

SAND2000-1765
Unlimited Release
Printed July 2000

Fast Grid Search Algorithm for Seismic Source Location

David F. Aldridge

Prepared by
Sandia National Laboratories
Albuquerque, New Mexico 87185 and Livermore, California 94550

Sandia is a multiprogram laboratory operated by Sandia Corporation, a Lockheed Martin Company, for the United States Department of Energy under Contract DE-AC04-94AL85000.

Sandia National Laboratories

Issued by Sandia National Laboratories, operated for the United States Department of Energy by Sandia Corporation.

Available to DOE and DOE contractors from
U.S. Department of Energy
Office of Scientific and Technical Information
P.O. Box 62
Oak Ridge, TN 37831

Telephone: (865)576-8401
Facsimile: (865)576-5728
E-Mail: reports@adonis.osti.gov
Online ordering: http://www.doe.gov/bridge

Available to the public from
U.S. Department of Commerce
National Technical Information Service
5285 Port Royal Rd
Springfield, VA 22161

Telephone: (800)553-6847
Facsimile: (703)605-6900
E-Mail: orders@ntis.fedworld.gov
Online order: http://www.ntis.gov/ordering.htm

SAND2000-1765
Unlimited Release
Printed July 2000

FAST GRID SEARCH ALGORITHM FOR SEISMIC SOURCE LOCATION

David F. Aldridge
Geophysical Technology Department
Sandia National Laboratories
P.O. Box 5800
Albuquerque, New Mexico, USA, 87185-0750

ABSTRACT

The spatial and temporal origin of a point seismic energy source are estimated by minimizing (in the weighted least squares sense) the misfit between observed and predicted arrival times at a set of receiver stations. A search is conducted for the best source position within a three-dimensional gridded volume of trial locations. During the search, rapid calculation of predicted arrival times is achieved by assuming a homogeneous and isotropic seismic velocity model. Compressional (P-wave) and shear (S-wave) seismic wave propagation speeds may be specified *a priori*, or optimum values are determined directly by the algorithm. Uncertainty in the final solution is assessed by analyzing contour plots of the arrival time misfit function in the vicinity of the absolute minimum. These plots also yield quantitative estimates of the resolving power of a given recording geometry.

CONTENTS

1.0 INTRODUCTION

Determining the location and origin time of a seismic energy source from a set of observed arrival times is a classic inverse problem in seismology. A successful solution of this problem is complicated by several factors, including:

1) The velocity distribution governing seismic energy propagation from source to receivers may be poorly known.
2) The observed arrival times, as well as the receiver locations, are subject to random and/or systematic errors.
3) The geometric distribution of receivers may be inadequate to resolve source location and origin time well.
4) The calculation of predicted arrival times at the receivers may be computationally demanding, even when the seismic velocity distribution is known (or assumed).
5) The inverse problem is (usually) nonlinear in the source position coordinates.

Many schemes for solving this problem assume a fixed seismic velocity model, and then seek the particular set of hypocentral parameters (source position coordinates x_s, y_s, z_s and origin time t_s) that minimizes a scalar measure of misfit between observed and predicted arrival times. The conventional approach entails iteratively updating an initial estimate of the hypocentral parameters until an acceptable data match is obtained (e.g., Buland, 1976; Thurber, 1985). More recently, a class of algorithms referred to as *search methods* have been developed (Sambridge and Kennett, 1986; Prugger and Gendzwill, 1988; Nelson and Vidale, 1990). These algorithms conduct a search (either systematic, guided, or probabilistic) over prescribed numerical ranges of the hypocentral parameters in order to locate the optimal set. Search methods possess some advantages compared with linearized iterative updating techniques. They are more apt to locate the absolute, rather than a relative, minimum of the misfit function. Calculation of arrival time derivatives is avoided, and sensitivity to initial estimates of the unknown parameters is much reduced. However, search methods can be computationally demanding. This is especially so for large numerical ranges in the unknown hypocentral parameters, and numerous predicted arrival times.

The present algorithm determines a seismic source position by conducting a systematic search through a three-dimensional rectangular grid of trial source locations. At each candidate location, predicted arrival times at a set of receivers are calculated. Computational simplicity and speed are maintained by assuming that source and receivers are situated within a homogeneous and isotropic medium characterized by P-wave speed α and S-wave speed β. Thus, the propagation time between any source-receiver pair is simply the intervening distance divided by the appropriate wavespeed. Arrival time misfit, defined as an L_2 norm of weighted residuals (differences between observed and predicted arrival times), is calculated for each trial source location. The particular position that minimizes the misfit is retained as the solution to the problem. The method accurately locates the global minimum of the misfit function provided i) the volume of parameter space searched encompasses this minimum, and ii) grid search increments are sufficiently small.

Adopting an L_2 norm (or least squares) misfit measure provides a certain benefit: the inverse problem becomes *linear* in the source origin time t_s and the wholespace slownesses (reciprocal velocities) $s_\alpha = 1/\alpha$ and $s_\beta = 1/\beta$. At each candidate source position, a simple 3×3 system of linear algebraic equations is solved to obtain the best fitting origin time and medium slownesses. Hence, there is no need to supply the location algorithm with a velocity estimate. However, *a priori* bounds on velocities (including restricting the two velocities to preferred values) are readily incorporated into the inversion scheme.

Although the assumption of a homogeneous and isotropic seismic velocity structure may seem severe, it is a reasonable approximation in some geologic situations, and is actually employed by some standard

microseismic event monitoring systems (e.g., McEvilly and Majer, 1982). To the extent that the actual seismic velocity distribution departs from this simple model, the inferred hypocentral parameters should be regarded as approximate, and subject to further refinement.

2.0 THEORY

2.1 Arrival Time Misfit

Suppose that a set of n arrival times t_i^{obs} ($i = 1 \rightarrow n$) are recorded due to a seismic wave propagating from a point source with unknown location (x_s, y_s, z_s) and origin time (t_s). These times may be a mixture of P-wave and S-wave arrivals, or wholly of one type. The arrivals are observed at a set of point receivers located at positions (x_i, y_i, z_i) ($i = 1 \rightarrow n$) in three-dimensional space. These positions need not be distinct; in particular, a given receiver may record both a P-wave and an S-wave arrival. The i^{th} predicted arrival time, calculated via any convenient seismic wave propagation theory, is designated t_i^{prd}. Then, the i^{th} arrival time residual is the difference $t_i^{obs} - t_i^{prd}$. An arrival time misfit function is defined as the (squared) L_2 norm of the weighted residuals:

$$M = \sum_{i=1}^{n} \left[w_i \left(t_i^{obs} - t_i^{prd} \right) \right]^2 , \tag{1}$$

where w_i are dimensionless weighting factors. A common situation involves uniform weighting ($w_i = w_0$ for $i = 1 \rightarrow n$). Nonuniform weighting may be employed to reduce the influence of data points with large residuals.

2.2 Predicted Arrival Time

For a homogeneous and isotropic medium characterized by P-wave slowness $s_\alpha = 1/\alpha$ and S-wave slowness $s_\beta = 1/\beta$, the i^{th} predicted arrival time is simply

$$t_i^{prd} = t_s + s_i d_i , \tag{2}$$

where d_i is the source-receiver distance:

$$d_i = \sqrt{(x_s - x_i)^2 + (y_s - y_i)^2 + (z_s - z_i)^2} , \tag{3}$$

and s_i is the slowness appropriate for the i^{th} observed arrival:

$$s_i = \begin{cases} s_\alpha & \text{if } t_i^{obs} \text{ is due to a P-wave} \\ s_\beta & \text{if } t_i^{obs} \text{ is due to an S-wave} \end{cases} . \tag{4}$$

2.3 Optimum Origin Time and Slowness

The common situation where all of the observed arrival times are associated with a *single* wave type (either P or S) is considered first. In this case, only one wholespace slowness can be determined.

2.3.1 One Wave Type

Taking $s_i = s$ (either s_α or s_β) and substituting equation (2) into equation (1) yields

$$M = \sum_{i=1}^{n} \left[w_i \left(t_i^{obs} - t_s - s d_i \right) \right]^2 . \tag{5}$$

Clearly, the misfit M is a quadratic function of the source initiation time t_s and wholespace slowness s. Partial derivatives of M with respect to these two parameters are

$$\frac{\partial M}{\partial t_s} = -2 \sum_{i=1}^{n} w_i^2 \left(t_i^{obs} - t_s - s d_i \right), \tag{6}$$

$$\frac{\partial M}{\partial s} = -2 \sum_{i=1}^{n} w_i^2 d_i \left(t_i^{obs} - t_s - s d_i \right). \tag{7}$$

Setting $\partial M/\partial t_s = \partial M/\partial s = 0$ yields the 2×2 linear algebraic system

$$\begin{bmatrix} \sum w_i^2 & \sum w_i^2 d_i \\ \sum w_i^2 d_i & \sum w_i^2 d_i^2 \end{bmatrix} \begin{bmatrix} t_s \\ s \end{bmatrix} = \begin{bmatrix} \sum w_i^2 t_i^{obs} \\ \sum w_i^2 d_i t_i^{obs} \end{bmatrix}, \tag{8}$$

with solution

$$t_s = \frac{\left(\sum w_i^2 d_i^2 \right) \left(\sum w_i^2 t_i^{obs} \right) - \left(\sum w_i^2 d_i \right) \left(\sum w_i^2 d_i t_i^{obs} \right)}{\left(\sum w_i^2 \right) \left(\sum w_i^2 d_i^2 \right) - \left(\sum w_i^2 d_i \right)^2}, \tag{9}$$

$$s = \frac{\left(\sum w_i^2 \right) \left(\sum w_i^2 d_i t_i^{obs} \right) - \left(\sum w_i^2 d_i \right) \left(\sum w_i^2 t_i^{obs} \right)}{\left(\sum w_i^2 \right) \left(\sum w_i^2 d_i^2 \right) - \left(\sum w_i^2 d_i \right)^2}. \tag{10}$$

All summations in equations (8) through (10) have index range $i = 1 \rightarrow n$. Expressions (9) and (10) represent the best fitting (in the weighted least squares sense) source origin time t_s and wholespace slowness s, for a given source location (x_s, y_s, z_s).

If the determinant of the linear system (8) vanishes, then the origin time and slowness are indeterminate. The determinant

$$\Delta = \left(\sum_{i=1}^{n} w_i^2 \right) \left(\sum_{i=1}^{n} w_i^2 d_i^2 \right) - \left(\sum_{i=1}^{n} w_i^2 d_i \right)^2 , \tag{11}$$

obviously vanishes in the two cases i) a single observed arrival time ($n = 1$), and ii) identical source-receiver distances ($d_i = d_0$ for $i = 1 \rightarrow n$). The first case is excluded *a priori* by the current source location algorithm. For $n > 1$, the determinant may be rewritten as

$$\Delta = \sum_{i=1}^{n-1} w_i^2 \sum_{j=i+1}^{n} w_j^2 (d_i - d_j)^2 \,. \tag{12}$$

The determinant is a linear a superposition of terms that are strictly non-negative. Thus, the *only* way Δ can vanish is for each term to individually vanish, implying $d_i = d_j$ for all i and j.

If all of the observed arrival times are identical ($t_i^{obs} = t_0$ for $i = 1 \rightarrow n$), then equations (9) and (10) give the interesting solution $t_s = t_0$ and $s = 0$. The misfit M reduces to zero. An exact fit to the observed arrival times is achieved with a source initiation time equal to the common observed arrival time, and a medium with infinite wavespeed. The source position is immaterial. This solution is, of course, nonphysical. Nevertheless, the situation $t_i^{obs} = t_0$ is theoretically possible, even with heterogeneous seismic velocity distribution.

In an actual field experiment, it is highly unlikely that all source-receiver distances or observed arrival times will be identical. Hence, the above two situations will rarely be encountered by the location algorithm.

2.3.2 Two Wave Types

In order to treat the case where a combination of compressional and shear arrival times are recorded, the misfit function (1) is rewritten as

$$M = \sum_{i=1}^{n_\alpha} \left[w_i \left(t_i^{obs} - t_s - s_\alpha d_i \right) \right]^2 + \sum_{i=n_\alpha+1}^{n} \left[w_i \left(t_i^{obs} - t_s - s_\beta d_i \right) \right]^2 \,. \tag{13}$$

where the first n_α ($1 \le n_\alpha < n$) arrivals are P-waves and the remaining n - n_α arrivals are S-waves. Setting $\partial M/\partial t_s = \partial M/\partial s_\alpha = \partial M/\partial s_\beta = 0$ gives the symmetric 3 × 3 system

$$\begin{bmatrix} \sum_{i=1}^{n} w_i^2 & \sum_{i=1}^{n_\alpha} w_i^2 d_i & \sum_{i=n_\alpha+1}^{n} w_i^2 d_i \\ \sum_{i=1}^{n_\alpha} w_i^2 d_i & \sum_{i=1}^{n_\alpha} w_i^2 d_i^2 & 0 \\ \sum_{i=n_\alpha+1}^{n} w_i^2 d_i & 0 & \sum_{i=n_\alpha+1}^{n} w_i^2 d_i^2 \end{bmatrix} \begin{bmatrix} t_s \\ s_\alpha \\ s_\beta \end{bmatrix} = \begin{bmatrix} \sum_{i=1}^{n} w_i^2 t_i^{obs} \\ \sum_{i=1}^{n_\alpha} w_i^2 d_i t_i^{obs} \\ \sum_{i=n_\alpha+1}^{n} w_i^2 d_i t_i^{obs} \end{bmatrix} . \tag{14}$$

The solution is:

$$t_s = \frac{1}{\Delta} \left\{ \left(\sum_{i=1}^{n_\alpha} w_i^2 d_i^2 \right) \left[\left(\sum_{i=1}^{n} w_i^2 t_i^{obs} \right) \left(\sum_{i=n_\alpha+1}^{n} w_i^2 d_i^2 \right) - \left(\sum_{i=n_\alpha+1}^{n} w_i^2 d_i t_i^{obs} \right) \left(\sum_{i=n_\alpha+1}^{n} w_i^2 d_i \right) \right] \right.$$

$$\left. - \left(\sum_{i=n_\alpha+1}^{n} w_i^2 d_i^2 \right) \left(\sum_{i=1}^{n_\alpha} w_i^2 d_i t_i^{obs} \right) \left(\sum_{i=1}^{n_\alpha} w_i^2 d_i \right) \right\}, \tag{15}$$

$$s_\alpha = \frac{1}{\Delta}\left\{\left(\sum_{i=1}^{n_\alpha} w_i^2 d_i\right)\left[\left(\sum_{i=n_\alpha+1}^{n} w_i^2 d_i t_i^{obs}\right)\left(\sum_{i=n_\alpha+1}^{n} w_i^2 d_i\right) - \left(\sum_{i=1}^{n} w_i^2 t_i^{obs}\right)\left(\sum_{i=n_\alpha+1}^{n} w_i^2 d_i^2\right)\right]\right.$$

$$\left. + \left(\sum_{i=1}^{n_\alpha} w_i^2 d_i t_i^{obs}\right)\left[\left(\sum_{i=1}^{n} w_i^2\right)\left(\sum_{i=n_\alpha+1}^{n} w_i^2 d_i^2\right) - \left(\sum_{i=n_\alpha+1}^{n} w_i^2 d_i\right)^2\right]\right\}, \tag{16}$$

$$s_\beta = \frac{1}{\Delta}\left\{\left(\sum_{i=n_\alpha+1}^{n} w_i^2 d_i\right)\left[\left(\sum_{i=1}^{n_\alpha} w_i^2 d_i t_i^{obs}\right)\left(\sum_{i=1}^{n_\alpha} w_i^2 d_i\right) - \left(\sum_{i=1}^{n} w_i^2 t_i^{obs}\right)\left(\sum_{i=1}^{n_\alpha} w_i^2 d_i^2\right)\right]\right.$$

$$\left. + \left(\sum_{i=n_\alpha+1}^{n} w_i^2 d_i t_i^{obs}\right)\left[\left(\sum_{i=1}^{n} w_i^2\right)\left(\sum_{i=1}^{n_\alpha} w_i^2 d_i^2\right) - \left(\sum_{i=1}^{n_\alpha} w_i^2 d_i\right)^2\right]\right\}, \tag{17}$$

where the determinant Δ is given by:

$$\Delta = \left[\left(\sum_{i=1}^{n} w_i^2\right)\left(\sum_{i=1}^{n_\alpha} w_i^2 d_i^2\right) - \left(\sum_{i=1}^{n_\alpha} w_i^2 d_i\right)^2\right]\left(\sum_{i=n_\alpha+1}^{n} w_i^2 d_i^2\right) - \left(\sum_{i=n_\alpha+1}^{n} w_i^2 d_i\right)^2\left(\sum_{i=1}^{n_\alpha} w_i^2 d_i^2\right). \tag{18}$$

The 3 × 3 system (14) exhibits indeterminacies that are similar to those of the 2 × 2 system (8). In particular, the determinant Δ vanishes if i) there is only one P-wave arrival and one S-wave arrival ($n = 2$ and $n_\alpha = 1$), and ii) all source-receiver distances are identical ($d_i = d_0$ for $i = 1 \rightarrow n$). Finally, if $t_i^{obs} = t_0$ for $i = 1 \rightarrow n$, then equations (15) through (18) yield the nonphysical solution $t_s = t_0$ and $s_\alpha = s_\beta = 0$.

3.0 ALGORITHM

3.1 Spatial Grid Search

A three-dimensional rectangular grid of trial source locations is established as follows:

Source x-coordinate: $x_s|_{\min} \Rightarrow x_s|_{\max}$ in increments δx_s
Source y-coordinate: $y_s|_{\min} \Rightarrow y_s|_{\max}$ in increments δy_s
Source z-coordinate: $z_s|_{\min} \Rightarrow z_s|_{\max}$ in increments δz_s

This grid should encompass the actual source position. Note that the grid intervals in the three coordinate directions need not be equal. Receivers are not restricted to reside within the search grid. If they do, they need not be located on gridpoints.

At each candidate source location, the set of source-receiver distances d_i, the optimum origin time t_s, optimum wholespace slownesses s_α and s_β, and the arrival time misfit M are determined. The particular

source position, origin time, and slownesses associated with the *minimum* misfit value are retained as the global solution to the problem. If higher spatial resolution is desired, a subsequent search can be conducted in the vicinity of this minimum point using finer grid increments. The example presented below adopts this strategy.

3.2 Constraints

Constrained inversions, where one or more parameters are restricted to known (or assumed) values, are readily performed. For example, if the seismic energy source resides on the earth's surface, then setting $z_s|_{min} = z_s|_{max} = 0$ reduces the spatial dimension of the search, and thus reduces algorithm execution time dramatically. Also, lower and upper bounds on source origin time and wholespace velocities can be imposed during the grid search. If a calculated origin time or slowness penetrates a bound, then the parameter is reset to the bounding value. Origin time and/or velocities can be constrained to *single* preferred values during the search merely by setting the relevant lower and upper bounds equal to each other.

3.2.1 One Wave Type

In the case where the wholespace velocity v is restricted to a single value, the source origin time is calculated via

$$t_s = \frac{\sum_{i=1}^{n} w_i^2 \left(t_i^{obs} - s d_i\right)}{\sum_{i=1}^{n} w_i^2}, \tag{19}$$

where $s = 1/v$. If the origin time t_s is constrained to a single value, then slowness s is calculated via

$$s = \frac{\sum_{i=1}^{n} w_i^2 d_i \left(t_i^{obs} - t_s\right)}{\sum_{i=1}^{n} w_i^2 d_i^2}. \tag{20}$$

Formulae (19) and (20) are derived by setting the appropriate partial derivative of the misfit measure M [equation (6) or (7)] equal to zero. If *both* origin time and slowness are constrained to *a priori* values, then the misfit norm (5) is evaluated directly with the specified values at each trial source location.

3.2.2 Two Wave Types

If the source activation time t_s is constrained to an *a priori* value, then the two medium slownesses are calculated via

$$s_\alpha = \frac{\sum_{i=1}^{n_\alpha} w_i^2 d_i \left(t_i^{obs} - t_s\right)}{\sum_{i=1}^{n_\alpha} w_i^2 d_i^2}, \qquad s_\beta = \frac{\sum_{i=n_\alpha+1}^{n} w_i^2 d_i \left(t_i^{obs} - t_s\right)}{\sum_{i=n_\alpha+1}^{n} w_i^2 d_i^2}. \tag{21a,b}$$

These formulae are obtained by setting $\partial M/\partial s_\alpha = \partial M/\partial s_\beta = 0$ where M is the misfit measure (13). If slowness s_β is constrained, then t_s and s_α are determined by solving the 2 × 2 system:

$$\begin{bmatrix} \sum_{i=1}^{n} w_i^2 & \sum_{i=1}^{n_\alpha} w_i^2 d_i \\ \sum_{i=1}^{n_\alpha} w_i^2 d_i & \sum_{i=1}^{n_\alpha} w_i^2 d_i^2 \end{bmatrix} \begin{bmatrix} t_s \\ s_\alpha \end{bmatrix} = \begin{bmatrix} \sum_{i=1}^{n} w_i^2 t_i^{obs} - s_\beta \sum_{i=n_\alpha+1}^{n} w_i^2 d_i \\ \sum_{i=1}^{n_\alpha} w_i^2 d_i t_i^{obs} \end{bmatrix}, \tag{22}$$

obtained via $\partial M/\partial t_s = \partial M/\partial s_\alpha = 0$. Similarly, if slowness s_α is constrained, then t_s and s_β are determined from the 2 × 2 system:

$$\begin{bmatrix} \sum_{i=1}^{n} w_i^2 & \sum_{i=n_\alpha+1}^{n} w_i^2 d_i \\ \sum_{i=n_\alpha+1}^{n} w_i^2 d_i & \sum_{i=n_\alpha+1}^{n} w_i^2 d_i^2 \end{bmatrix} \begin{bmatrix} t_s \\ s_\beta \end{bmatrix} = \begin{bmatrix} \sum_{i=1}^{n} w_i^2 t_i^{obs} - s_\alpha \sum_{i=1}^{n_\alpha} w_i^2 d_i \\ \sum_{i=n_\alpha+1}^{n} w_i^2 d_i t_i^{obs} \end{bmatrix}, \tag{23}$$

obtained via $\partial M/\partial t_s = \partial M/\partial s_\beta = 0$. If *both* slownesses are constrained, then origin time is calculated by:

$$t_s = \frac{\sum_{i=1}^{n} w_i^2 \left(t_i^{obs} - s_i d_i \right)}{\sum_{i=1}^{n} w_i^2}, \tag{24}$$

where s_i is given by equation (4).

4.0 EXAMPLE

The example involves a set of P-wave traveltimes generated by an explosion source with a known location. Figure 1 illustrates the distribution of 16 receivers (indicated by triangles) projected onto horizontal (xy) and vertical (xz) planes. The source position is depicted on each section with a circle. Observed arrival times (referenced to a presumed source origin time of 0.0 ms) are also displayed; these range from 58.3 ms to 226.2 ms, and are estimated to have picking errors of about ±20 ms. Four different inversions of these data presented below utilize uniform weighting of arrival times.

4.1 Unconstrained Search

In the first inversion, an initial estimate of the source location is determined with the relatively coarse spatial grid interval of 10 m. Very wide (and hence ineffectual) bounds on origin time and P-wave speed are imposed during this search. Subsequent reduction of the grid interval to 2 m yields the more refined solution

$x_s = 195702$ m, $y_s = 252174$ m, $z_s = 270$ m, $t_s = -24.03$ ms, $\alpha = 2291.5$ m/s.

The rms arrival time misfit is 13.02 ms, and the residuals (plotted in the bottom panel of figure 1) range from –22.87 ms to +23.28 ms and have zero mean. Squares plotted on the horizontal and vertical sections of figure 1 indicate the estimated source position. Although the epicentral coordinates are reasonably correct (~51 m from the known location), the source depth is seriously overestimated (172 m too deep).

4.2 Constrained Velocity

In the second inversion, wholespace P-wave speed is constrained to equal $\alpha = 2875$ m/s. This particular value is inferred by fitting a straight line to a plot of arrival time vs. source-receiver distance. A grid search using a 2 m spatial interval returns the solution

$$x_s = 195714 \text{ m}, \qquad y_s = 252156 \text{ m}, \qquad z_s = 138 \text{ m}, \qquad t_s = +24.54 \text{ ms},$$

with an rms arrival time misfit of 13.88 ms. Squares plotted on the horizontal and vertical sections of figure 2 give the estimated source position. Compared with the first inversion, this solution exhibits a slight degradation in epicentral accuracy (to ~58 m) but a greatly improved depth estimate (40 m below the correct depth). Arrival time residuals (plotted in the bottom panel of figure 2) range from –25.62 ms to +24.10 ms and have zero mean.

4.3 Constrained Origin Time

Curiously, the estimated source origin times for the first two inversions have approximately the same magnitude, but opposite sign. The third inversion entails constraining the origin time to $t_s = 0.00$ ms, since arrival times at the receivers are measured with respect to the known instant of source detonation. A grid search on a 2 m interval gives the solution

$$x_s = 195706 \text{ m}, \qquad y_s = 252170 \text{ m}, \qquad z_s = 214 \text{ m}, \qquad \alpha = 2492.6 \text{ m/s},$$

and is plotted in figure 3. The rms arrival time misfit is 13.12 ms, with minimum and maximum residuals of –23.95 ms and +22.43 ms, respectively, and mean equal to –0.1 ms. Solution accuracy is intermediate between the first two inversions; epicentral error is ~53 m and depth error is 116 m.

4.4 Constrained Velocity and Origin Time

Finally, constraining *both* the wholespace velocity (to 2875 m/s) and source origin time (to 0.00 ms) yields the solution

$$x_s = 195730 \text{ m}, \qquad y_s = 252118 \text{ m}, \qquad z_s = 248 \text{ m},$$

with an rms arrival time misfit of 15.47 ms. Minimum and maximum residuals are –26.31 ms and +35.15 ms, and the mean residual equals +1.2 ms. Figure 4 depicts this solution, which appears inferior to the previous three inversions. Epicentral error is ~81 m and depth error is 150 m.

In all four inversions, the spatial grid comprised 101 × 101 × 151 = 1,540,351 points, and the search required about 3 seconds of execution time (including all input/output) on a standard (but currently outdated) serial computer.

5.0 UNCERTAINTY and RESOLUTION

5.1 Field P-Wave dataset

The uncertainty and/or non-uniqueness of a solution are quantified by depicting the arrival time misfit as a function of the four hypocentral parameters (x_s, y_s, z_s, t_s) near the minimum point. Contour plots of misfit as a function of two selected parameters are simple to construct. Since there are four inversion parameters, there are six distinct parameter pairs that can form the independent variables of a contour plot. Figures 5 and 6 illustrate the quantity

$$E = \sqrt{M \Big/ \sum_{i=1}^{n} w_i^2} \ , \tag{25}$$

contoured in 5 ms intervals above these six "hyperplanes" through 4D model space. The origin of each plot (indicated by +) refers to the parameter set recovered in the first inversion described above (i.e., grid search with unconstrained slowness and origin time). Hence, rms arrival time misfit equals 13.02 ms at this point.

In all cases, as the hypocentral parameters deviate from the best fitting solution, the rms misfit E increases monotonically. With regard to variations in source position coordinates, the misfit exhibits a fairly broad and "bowl-shaped" character in the vicinity of the minimum (figure 5). When the source origin time t_s is varied, the minimum is narrow and elongate (figure 6). Errors in the picked arrival times and the assumed velocity model imply that all parameter pairs contained within a selected contour (say, the 20 ms contour) should be considered acceptable solutions to this location/origin time problem. In particular, source depth z_s and origin time t_s are not well-resolved. The depth may vary through a broad range of values near the minimum point, with very little effect on the overall arrival time misfit, *if* the origin time undergoes a simultaneous, but correlated, change.

Similar plots quantifying source location uncertainty (in space, but not in time) are presented by Buland (1976), Sambridge and Kennett (1986), and Prugger and Gendzwill (1988).

5.2 Synthetic P-Wave and S-Wave Datasets

The resolving power of the recording geometry in the above field data example can be examined by generating synthetic arrival time datasets using the known source and receiver coordinates. Hence, a set of 16 noise-free P-wave arrival times are calculated with hypocentral parameters and compressional wavespeed given by

$$x_s = 195656 \text{ m}, \qquad y_s = 252152 \text{ m}, \qquad z_s = 98 \text{ m}, \qquad t_s = 0.0 \text{ ms}, \qquad \alpha = 2291.5 \text{ m/s}.$$

The P-wave speed is the best-fitting value obtained in the first inversion described above. Since the synthetic arrival times are not contaminated with picking errors, the grid search inversion algorithm recovers the above parameters exactly.

Figures 7 and 8 display the rms arrival time misfit (25) contoured above the six hyperplanes through 4D model space. The origin of each plot (+ symbol) refers to the known spatial and temporal coordinates of the source. Hence, rms misfit E equals 0.0 ms at +. These plots represent "the best that can be achieved" with the given recording geometry and inversion algorithm, because all arrival times are computed from a model that agrees precisely with the algorithmic assumption (i.e., homogeneous and isotropic wholespace). In particular, the figures imply that source epicentral coordinates (x_s, y_s) and origin time t_s

can be localized reasonably well, provided rms picking error does not exceed about 5 ms. However, source depth z_s cannot be resolved adequately at the same error level. Reduced depth resolution is a common feature of seismic source location algorithms, when all receiver stations are distributed on or near the earth's surface. Plot scales and contour intervals (5 ms) in figures 7 and 8 are identical to those used for figures 5 and 6 in order to facilitate comparisons.

Finally, in order to illustrate the benefits of including shear wave arrivals in the inversion scheme, a combined set of P-wave and S-wave arrival times are calculated using the known source and receiver locations. Each receiver station is assumed to record both a P-wave and an S-wave; hence, there are 32 noise-free synthetic arrival times. The shear wavespeed is taken to be $\beta = 1145.75$ m/s (one half of the P-wave speed).

Figures 9 and 10 illustrate the contoured rms arrival time misfit, plotted at the same scales and contour interval as in figures 7 and 8. The contours close more tightly about the origin, indicating that simultaneous inversion of combined P-wave and S-wave arrivals yields a superior hypocentral solution. This agrees with previous observations by Buland (1976) and Rabinowitz and Steinberg (1990). However, some of the improvement in the present case may be due to the increased number of arrival times (32 *vs.* 16).

6.0 CONCLUSION

The spatial and temporal origin of a seismic energy source are estimated with a fast grid search technique. This approach has greater likelihood of finding the global minimum of the arrival time misfit function compared with conventional linearized iterative methods. Assumption of a homogeneous and isotropic seismic velocity model allows for extremely rapid computation of predicted arrival times, but probably limits application of the method to certain geologic environments and/or recording geometries.

Contour plots of the arrival time misfit function in the vicinity of the global minimum are extremely useful for i) quantifying the uncertainty of an estimated hypocenter solution, and ii) analyzing the resolving power of a given recording configuration. In particular, simultaneous inversion of both P-wave and S-wave arrival times appears to yield a superior solution, in the sense of being more precisely localized in space and time.

Future research with this algorithm may involve i) investigating the utility of nonuniform residual weighting schemes, ii) incorporating linear and/or layered velocity models into the calculation of predicted arrival times, and iii) applying it toward rational design of microseismic monitoring networks.

7.0 REFERENCES

Buland, R., 1976, The mechanics of locating earthquakes: Bulletin of the Seismological Society of America, **66**, 173-187.

McEvilly, T.V., and Majer, E.L., 1982, ASP: an automated seismic processor for microearthquake networks: Bulletin of the Seismological Society of America, **72**, 303-325.

Nelson, G.D., and Vidale, J.E., 1990, Earthquake locations by 3-D finite-difference travel times: Bulletin of the Seismological Society of America, **80**, 395-410.

Prugger, A.F., and Gendzwill, D.J., 1988, Microearthquake location: a nonlinear approach that makes use of a simplex stepping procedure: Bulletin of the Seismological Society of America, **78**, 799-815.

Sambridge, M.S., and Kennett, B.L.N., 1986, A novel method of hypocentre location: Geophysical Journal of the Royal Astronomical Society, **87**, 679-697.

Rabinowitz, N., and Steinberg, D.M., 1990, Optimal configuration of a seismographic network: a statistical approach: Bulletin of the Seismological Society of America, **80**, 187-196.

Thurber, C.H., 1985, Nonlinear earthquake location: theory and examples: Bulletin of the Seismological Society of America, **75**, 779-790.

8.0 FIGURES

Figure 1: Inversion results for an unconstrained grid search. The upper two panels illustrate the geometric distribution of 16 receivers (triangles) and the known source (circle) projected onto horizontal (*xy*) and vertical (*xz*) planes, respectively. The estimated source location is indicated by squares on each panel. The bottom two panels depict the observed P-wave arrival times and residuals, respectively.

Figure 2: Inversion results for a grid search with constrained P-wave speed. Panels display similar information as figure 1.

Figure 3: Inversion results for a grid search with constrained origin time. Panels display similar information as figure 1.

Figure 4: Inversion results for a grid search with constrained P-wave speed and origin time. Panels display similar information as figure 1.

Figure 5: Contour plots of the rms arrival time misfit on three orthogonal spatial planes passing through the source position estimated in the first example (i.e., unconstrained grid search of figure 1). The origin of each plot (+ symbol) refers to the derived source location (x_s, y_s, z_s) where the rms arrival time misfit equals 13.02 ms. Contour interval equals 5 ms.

Figure 6: Contour plots of the rms arrival time misfit on three "hyperplanes" passing through the hypocenter parameter solution of the first example (i.e., unconstrained grid search). Origin of each plot (+ symbol) refers to the derived hypocentral solution (x_s, y_s, z_s, t_s) where the rms arrival time misfit equals 13.02 ms. Contour interval equals 5 ms.

Figure 7: Contour plots of the rms arrival time misfit on three orthogonal spatial planes passing through the known source position (+ symbol). 16 synthetic noise-free P-wave arrivals are inverted. Contour interval equals 5 ms.

Figure 8: Contour plots of the rms arrival time misfit on three hyperplanes passing through the known hypocenter (+ symbol). 16 synthetic noise-free P-wave arrivals are inverted. Contour interval equals 5 ms.

Figure 9: Contour plots of the rms arrival time misfit on three orthogonal spatial planes passing through the known source position (+ symbol). 32 synthetic noise-free arrival times (16 P-waves and 16 S-waves) are inverted. Contour interval equals 5 ms.

Figure 10: Contour plots of the rms arrival time misfit on three hyperplanes passing through the known hypocenter (+ symbol). 32 synthetic noise-free arrival times (16 P-waves and 16 S-waves) are inverted. Contour interval equals 5 ms.

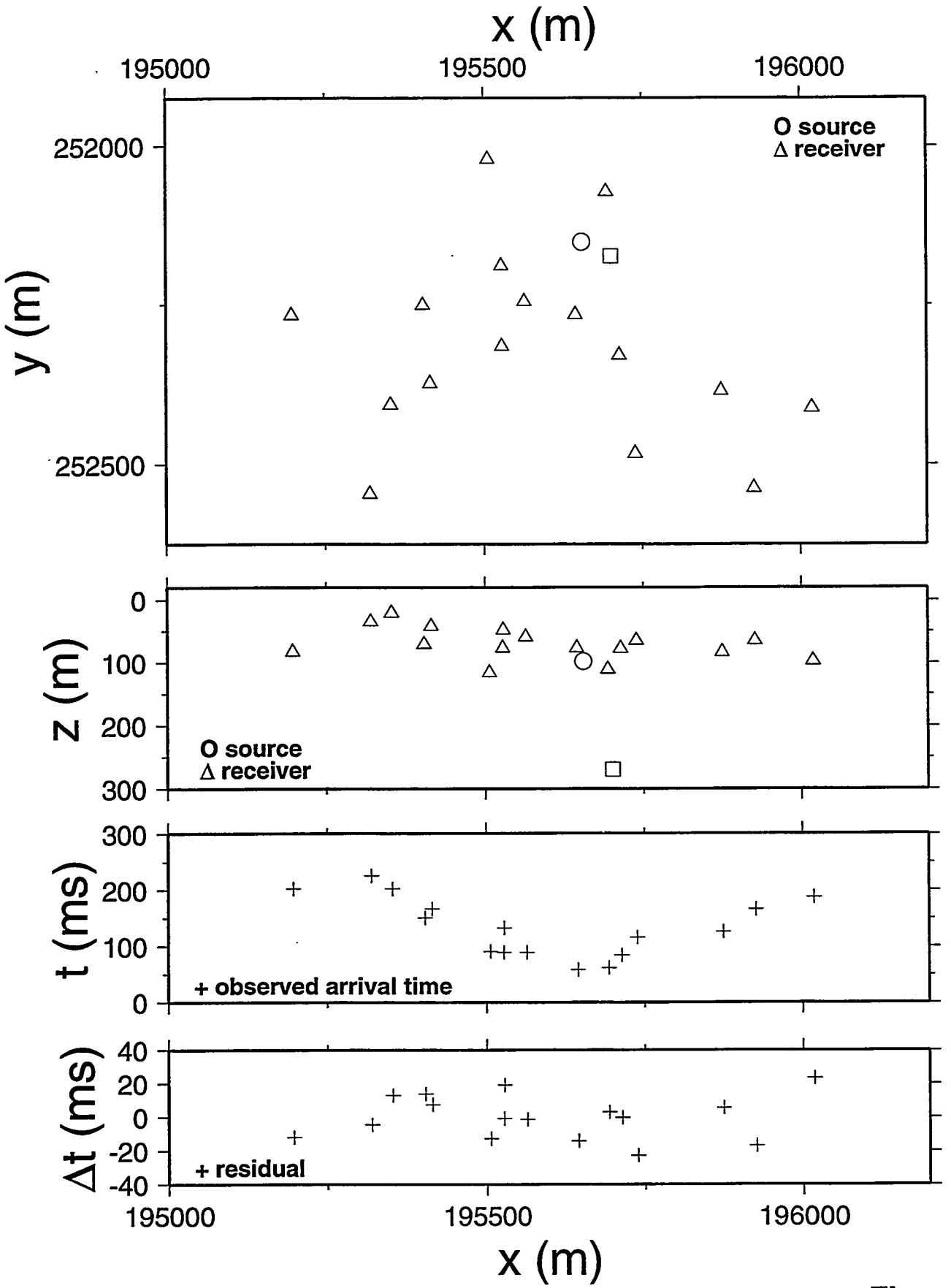
x (m)
195000
195500
196000
252000
252500
y (m)
O source
Δ receiver
z (m)
0
100
200
300
O source
Δ receiver
t (ms)
300
200
100
0
+ observed arrival time
Δt (ms)
40
20
0
-20
-40
+ residual
195000
195500
196000
x (m)

Figure 1

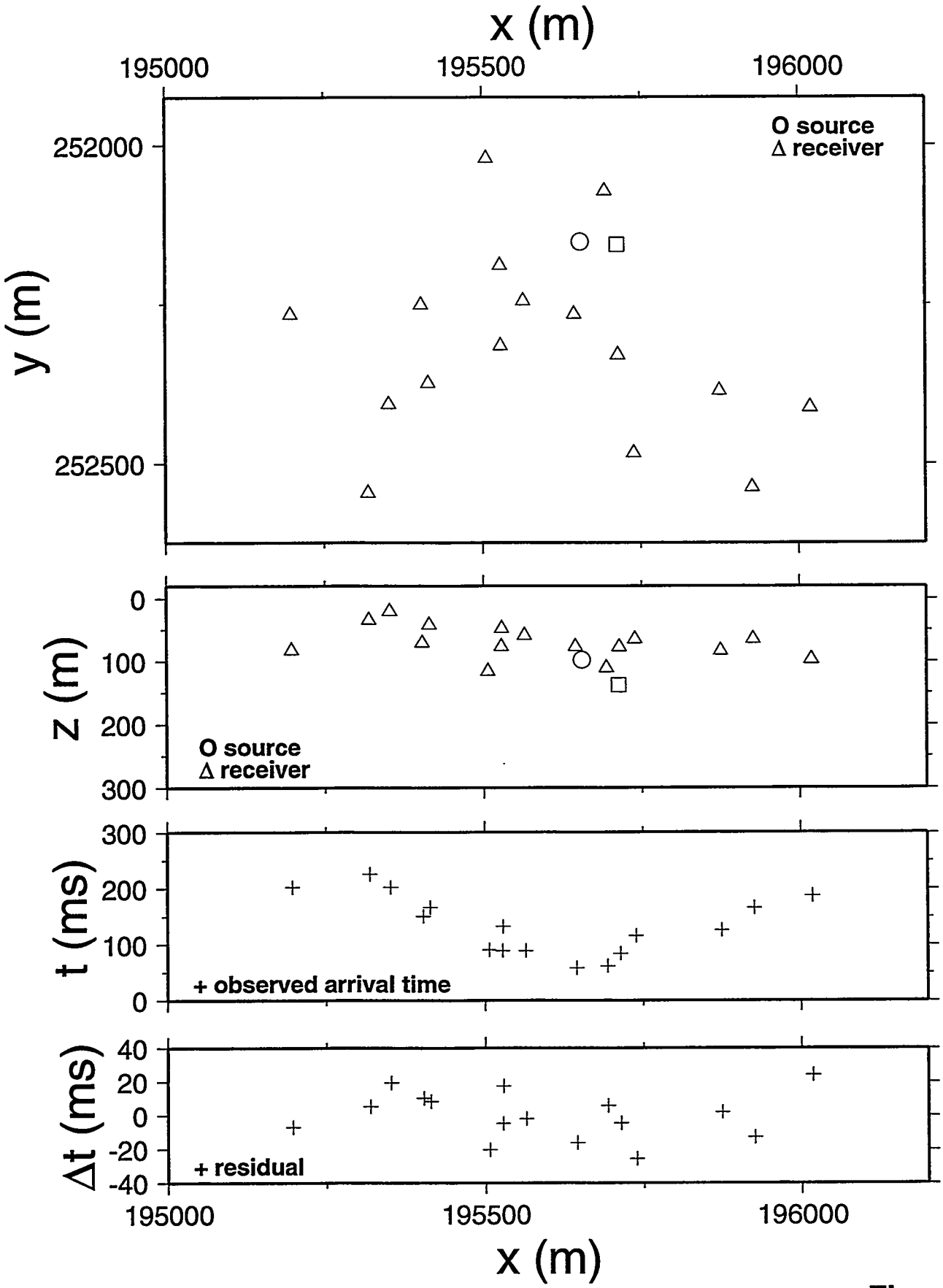
x (m)
195000
195500
196000
252000
252500
y (m)
O source
Δ receiver
z (m)
0
100
200
300
O source
Δ receiver
t (ms)
300
200
100
0
+ observed arrival time
Δt (ms)
40
20
0
-20
-40
+ residual
195000
195500
196000
x (m)

Figure 2

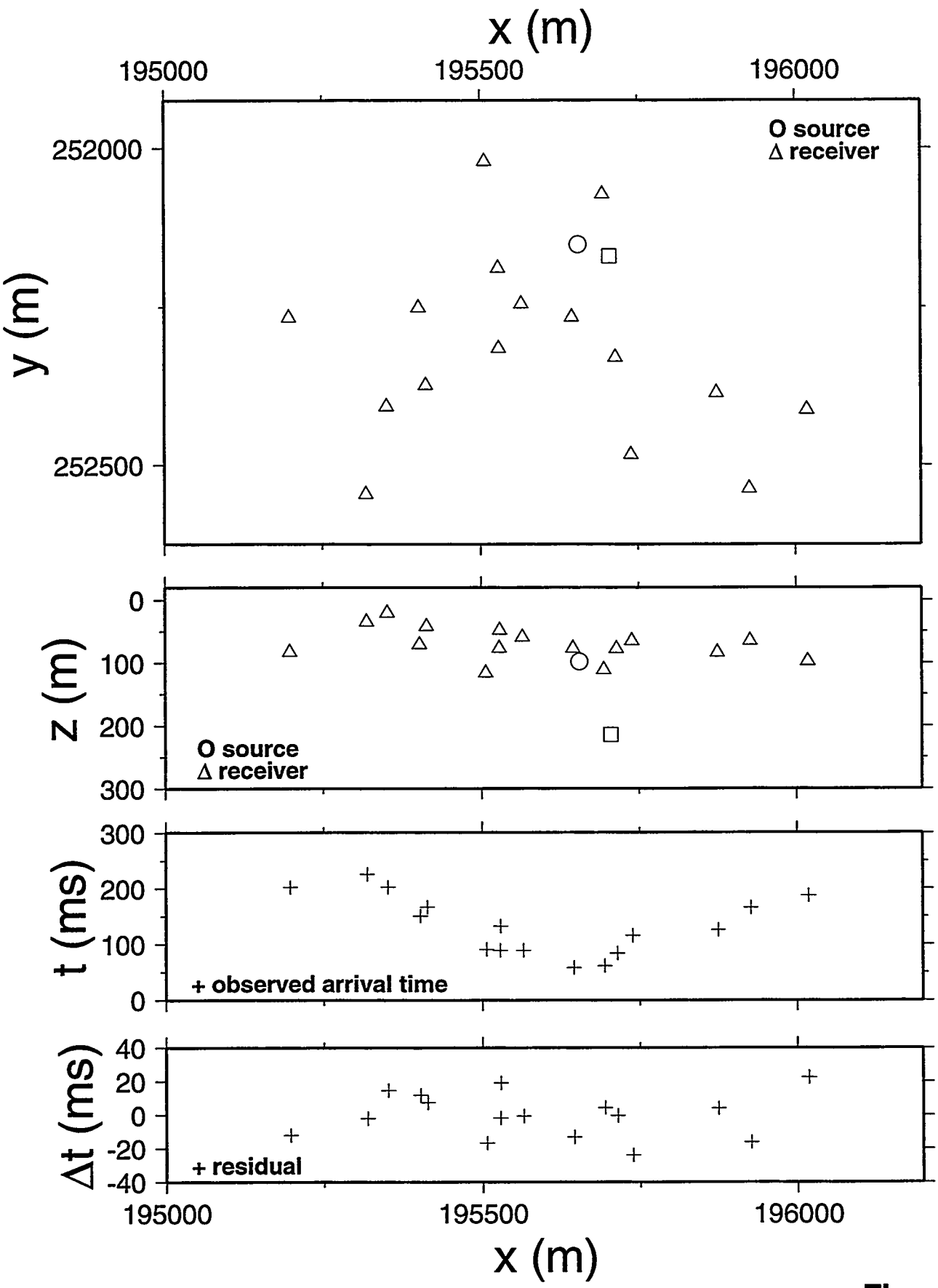
x (m)
195000
195500
196000
252000
252500
y (m)
O source
Δ receiver
z (m)
0
100
200
300
O source
Δ receiver
t (ms)
300
200
100
0
+ observed arrival time
Δt (ms)
40
20
0
-20
-40
+ residual
195000
195500
196000
x (m)

Figure 3

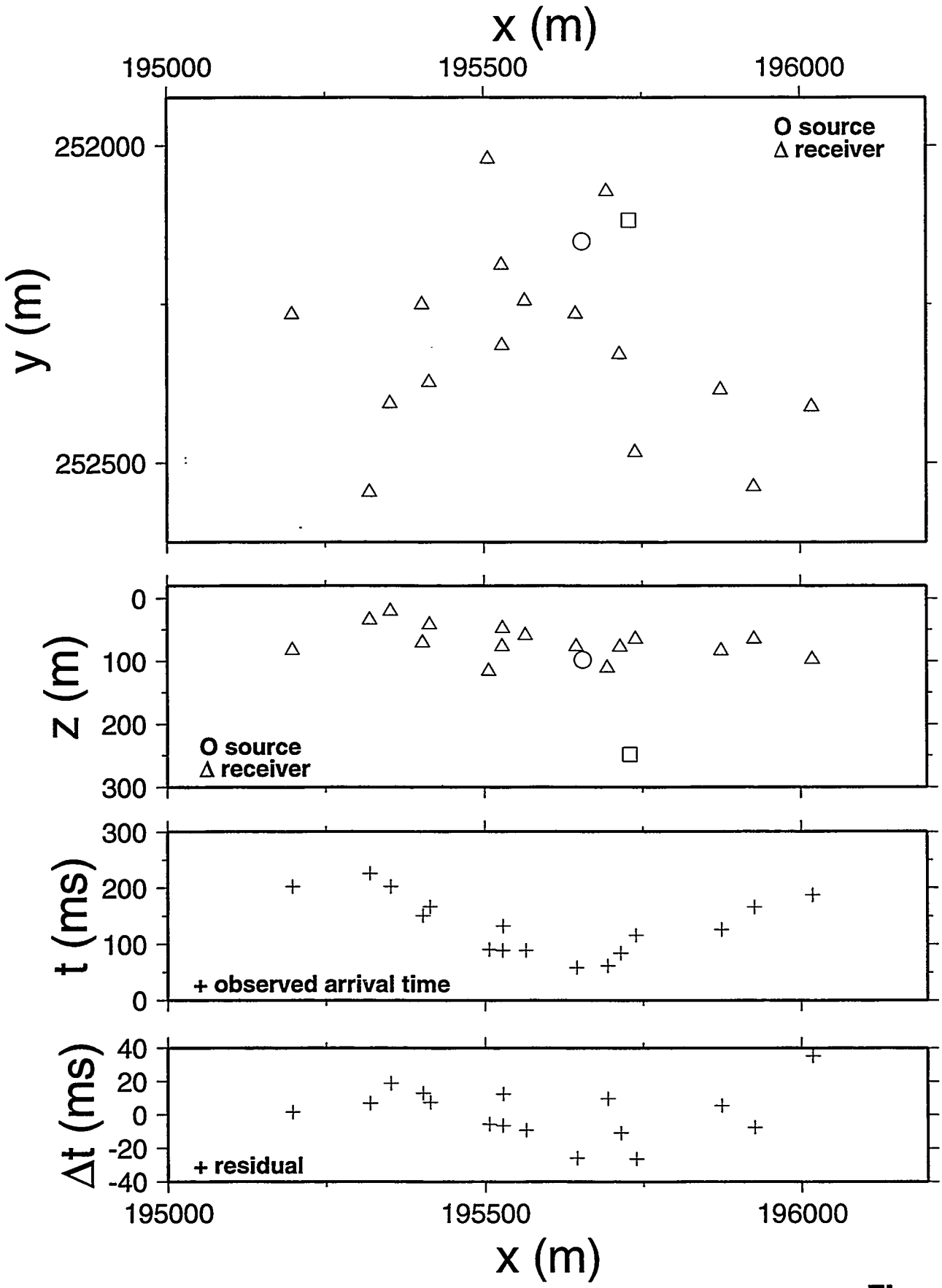
x (m)
195000
195500
196000
252000
252500
y (m)
O source
Δ receiver
z (m)
0
100
200
300
O source
Δ receiver
t (ms)
300
200
100
0
+ observed arrival time
Δt (ms)
40
20
0
-20
-40
+ residual
195000
195500
196000
x (m)

Figure 4

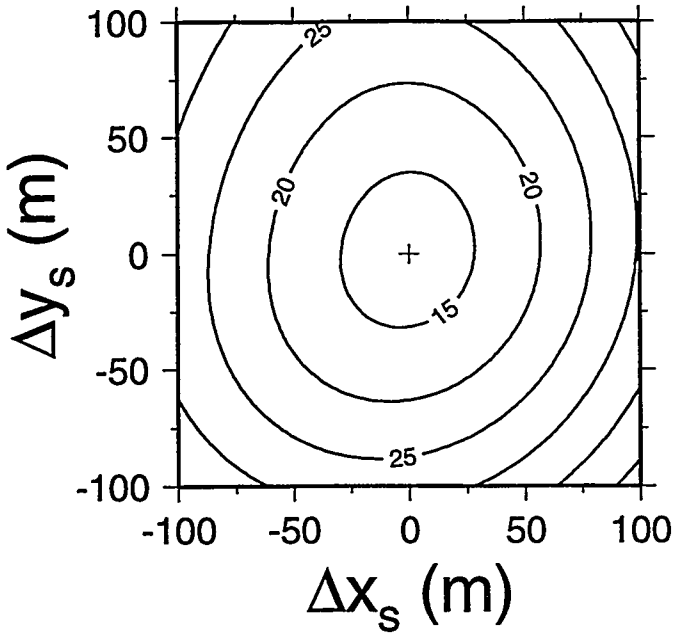
100
50
0
-50
-100
-100
-50
0
50
100
Δy_s (m)
Δx_s (m)
25
20
20
15
25

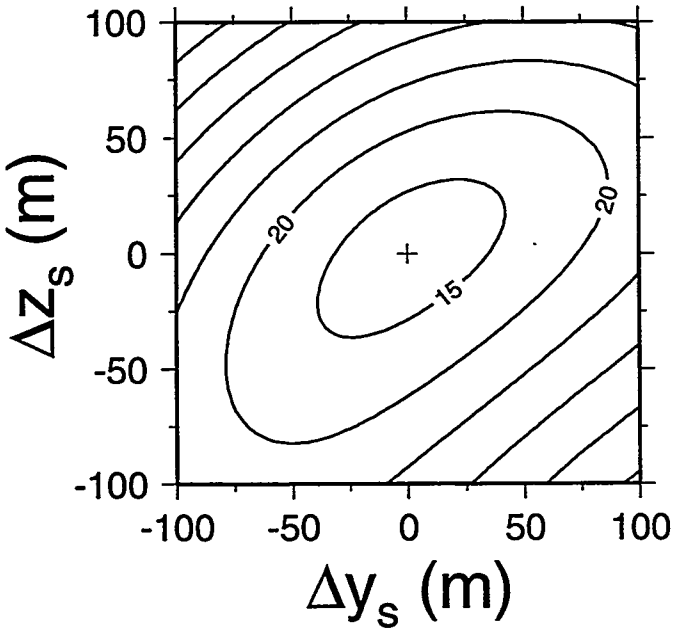
100
50
0
-50
-100
-100
-50
0
50
100
Δz_s (m)
Δy_s (m)
20
20
15

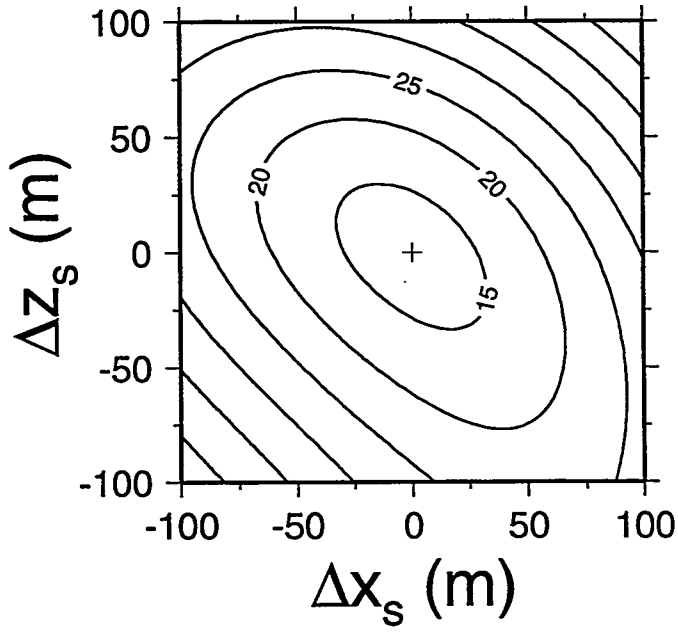
100
50
0
-50
-100
-100
-50
0
50
100
Δz_s (m)
Δx_s (m)
25
20
20
15

Figure 5

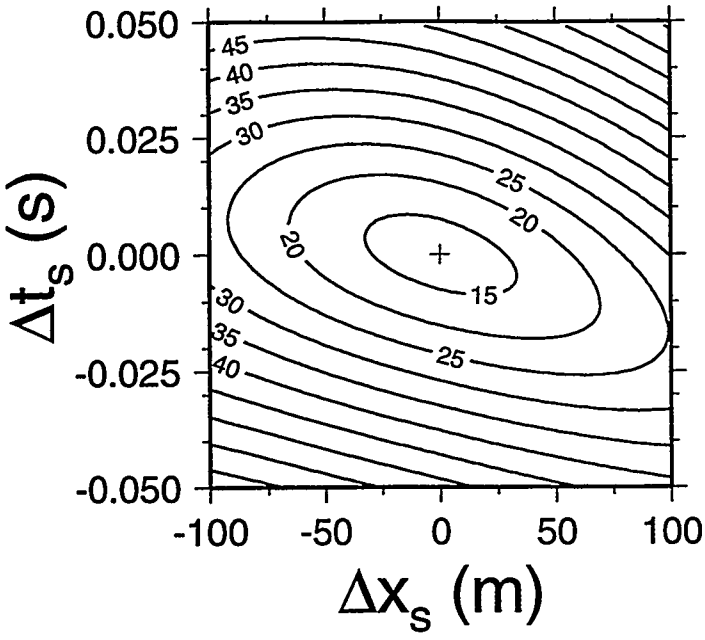
0.050
0.025
0.000
-0.025
-0.050
Δt_s (s)
45
40
35
30
25
20
15
-100
-50
0
50
100
Δx_s (m)

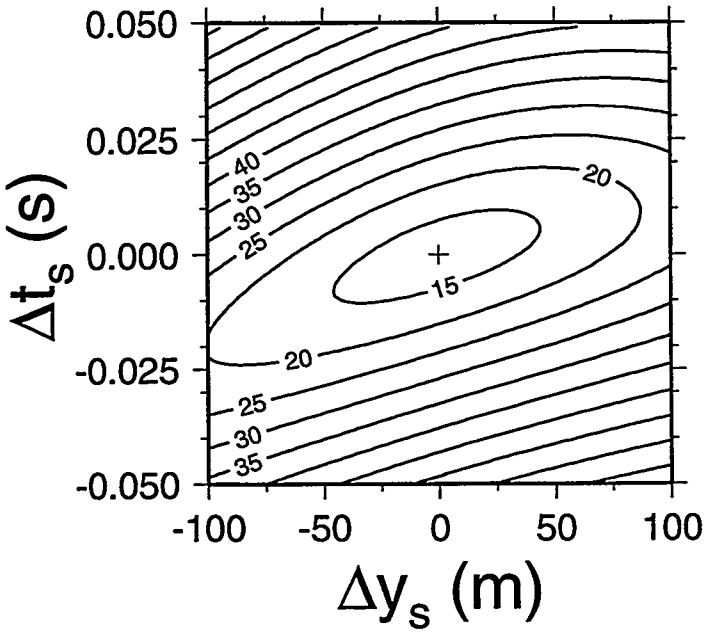
0.050
0.025
0.000
-0.025
-0.050
Δt_s (s)
40
35
30
25
20
15
-100
-50
0
50
100
Δy_s (m)

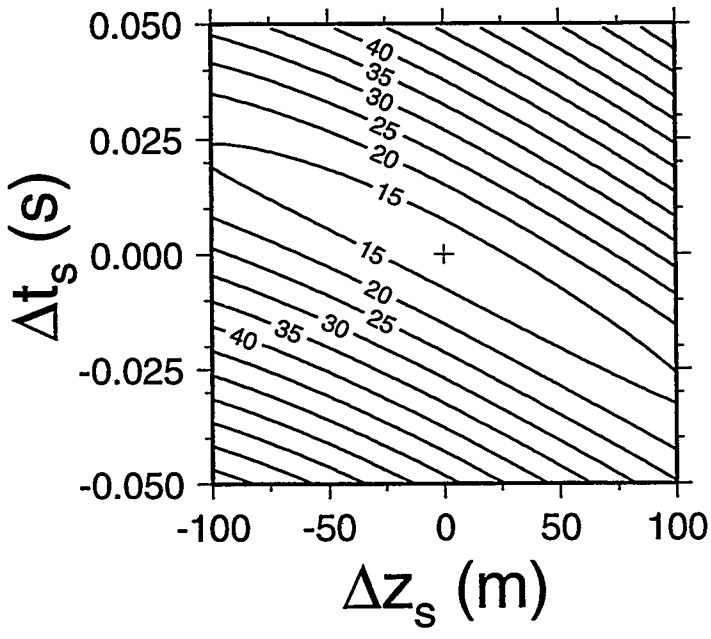
0.050
0.025
0.000
-0.025
-0.050
Δt_s (s)
40
35
30
25
20
15
-100
-50
0
50
100
Δz_s (m)

Figure 6

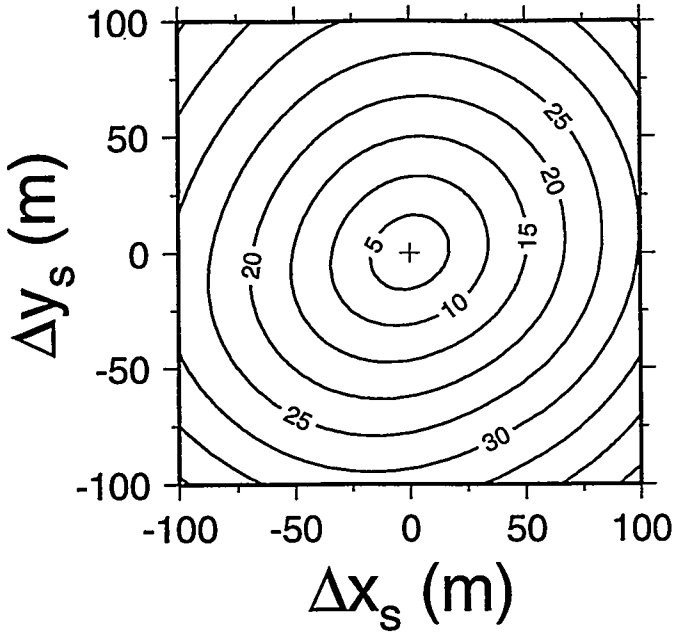
100
50
0
-50
-100
-100
-50
0
50
100
Δy_s (m)
Δx_s (m)
5
10
15
20
25
30

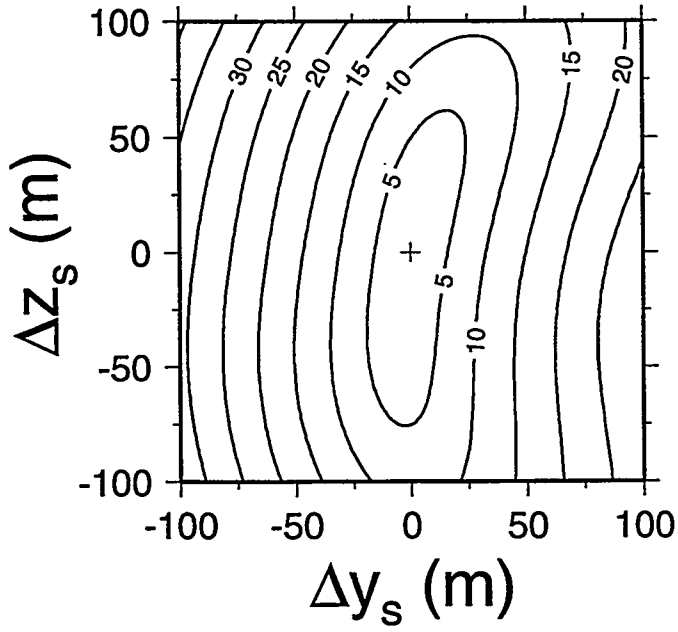
100
50
0
-50
-100
-100
-50
0
50
100
Δz_s (m)
Δy_s (m)
5
10
15
20
25
30

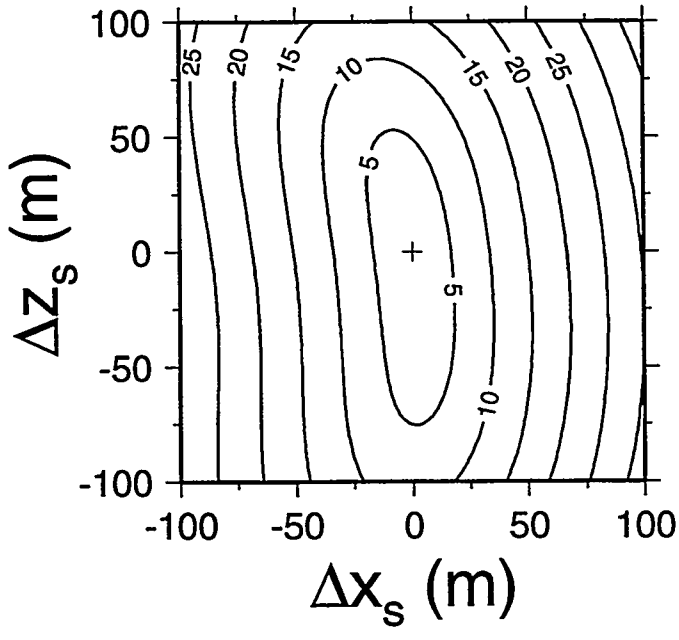
100
50
0
-50
-100
-100
-50
0
50
100
Δz_s (m)
Δx_s (m)
5
10
15
20
25

Figure 7

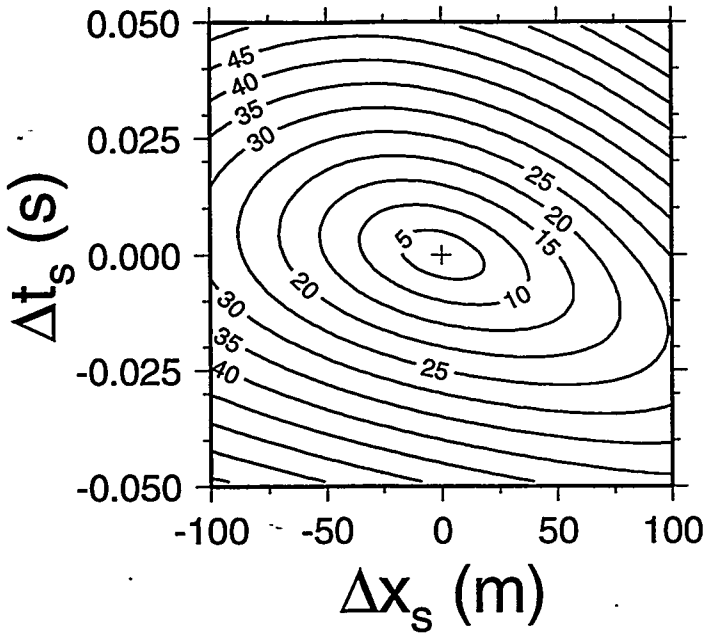
0.050
0.025
0.000
-0.025
-0.050
Δt_s (s)
-100
-50
0
50
100
Δx_s (m)
45
40
35
30
25
20
15
10
5

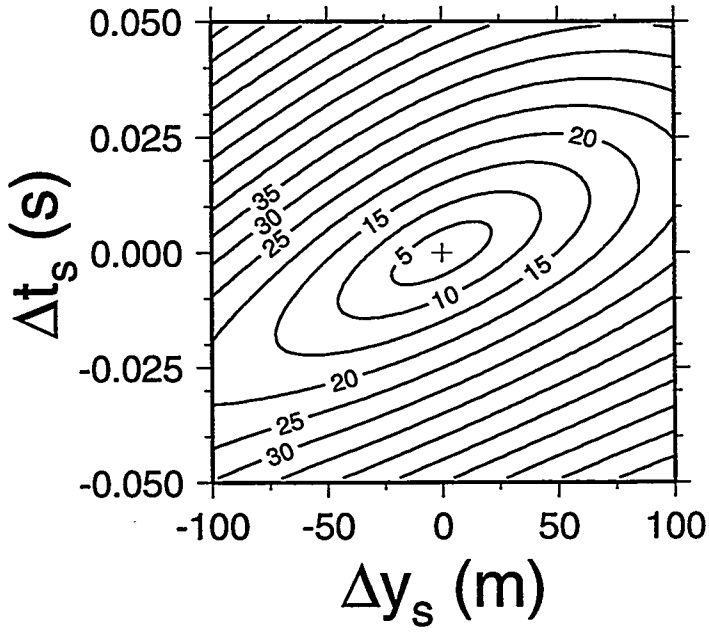
0.050
0.025
0.000
-0.025
-0.050
Δt_s (s)
-100
-50
0
50
100
Δy_s (m)
35
30
25
20
15
10
5

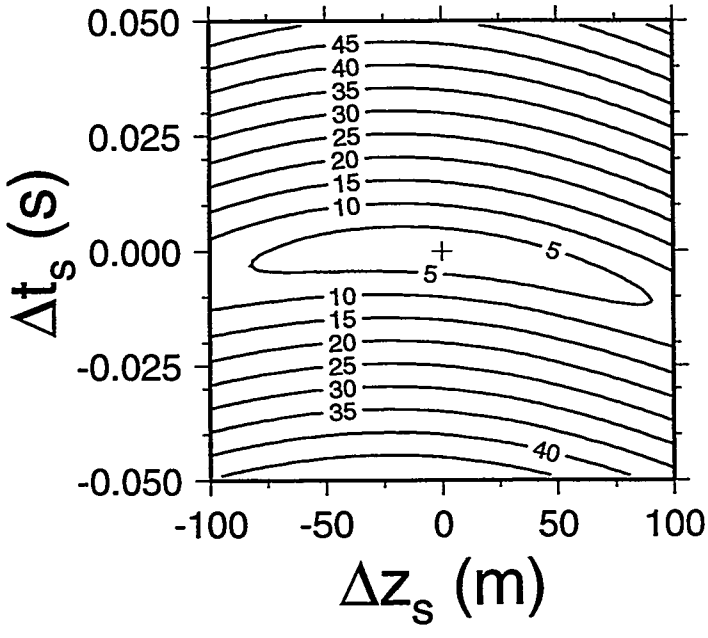
0.050
0.025
0.000
-0.025
-0.050
Δt_s (s)
-100
-50
0
50
100
Δz_s (m)
45
40
35
30
25
20
15
10
5

Figure 8

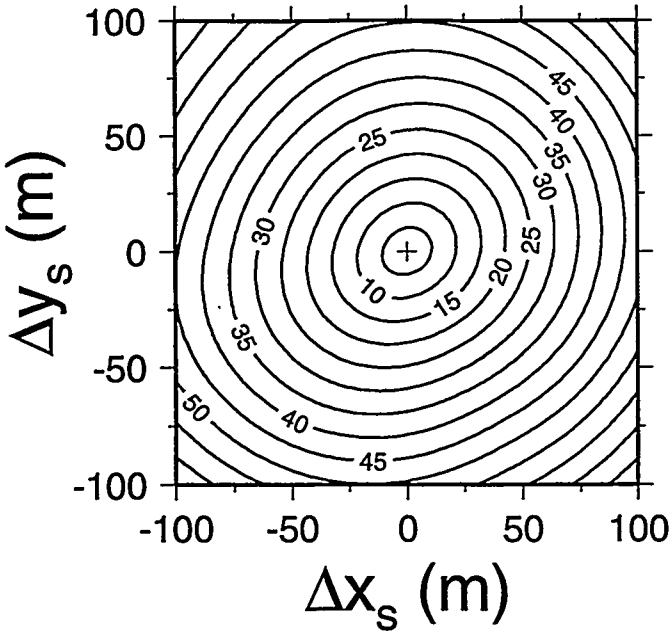
100
50
0
-50
-100
-100
-50
0
50
100
Δy_s (m)
Δx_s (m)
10
15
20
25
30
35
40
45
50

Figure 9

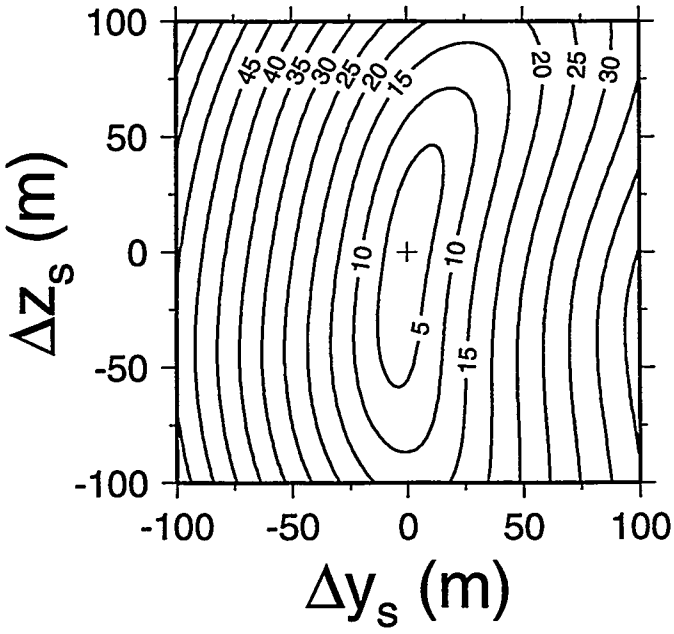
100
50
0
-50
-100
-100
-50
0
50
100
Δz_s (m)
Δy_s (m)
5
10
15
20
25
30
35
40
45

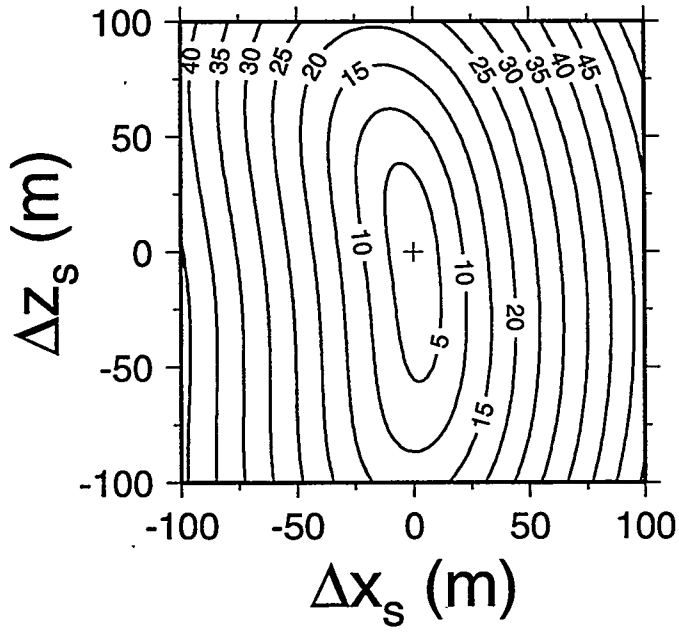
100
50
0
-50
-100
-100
-50
0
50
100
Δz_s (m)
Δx_s (m)
5
10
15
20
25
30
35
40
45

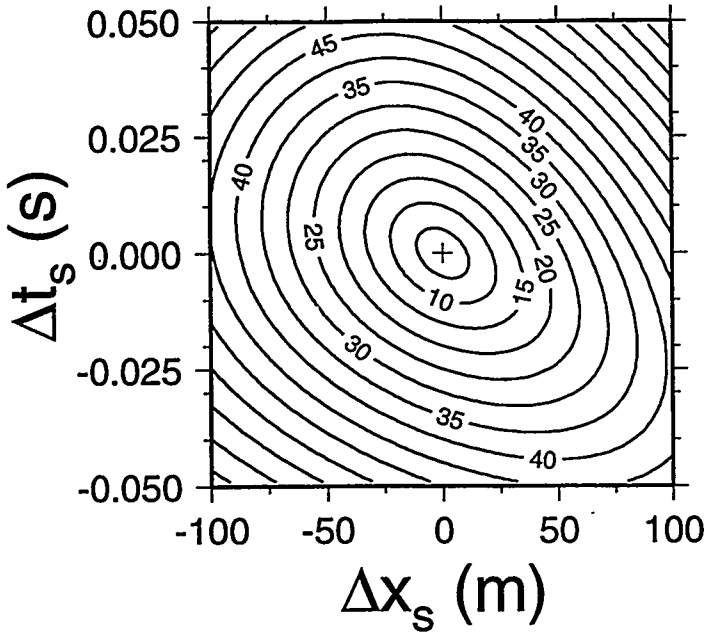
0.050
0.025
0.000
-0.025
-0.050
Δt_s (s)
-100
-50
0
50
100
Δx_s (m)
45
35
40
35
30
25
20
15
10
25
30
35
40

Figure 10

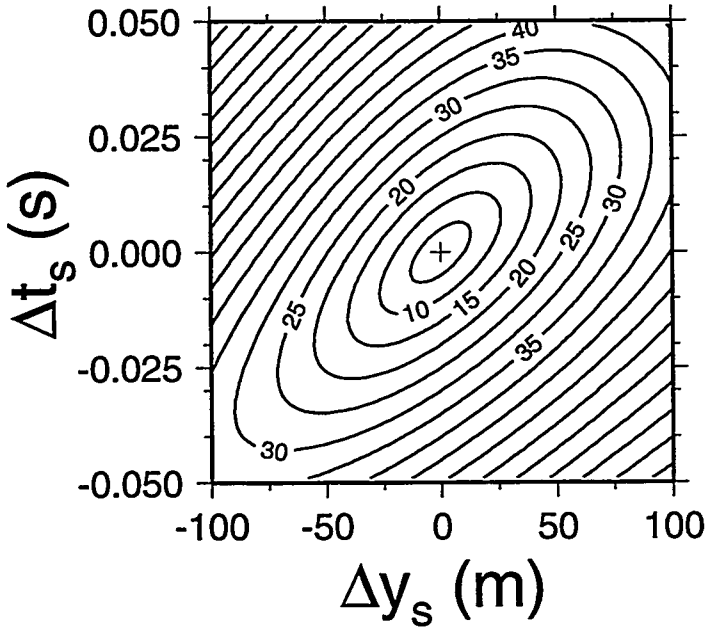
0.050
0.025
0.000
-0.025
-0.050
Δt_s (s)
-100
-50
0
50
100
Δy_s (m)
40
35
30
20
25
30
25
10
15
20
35
30

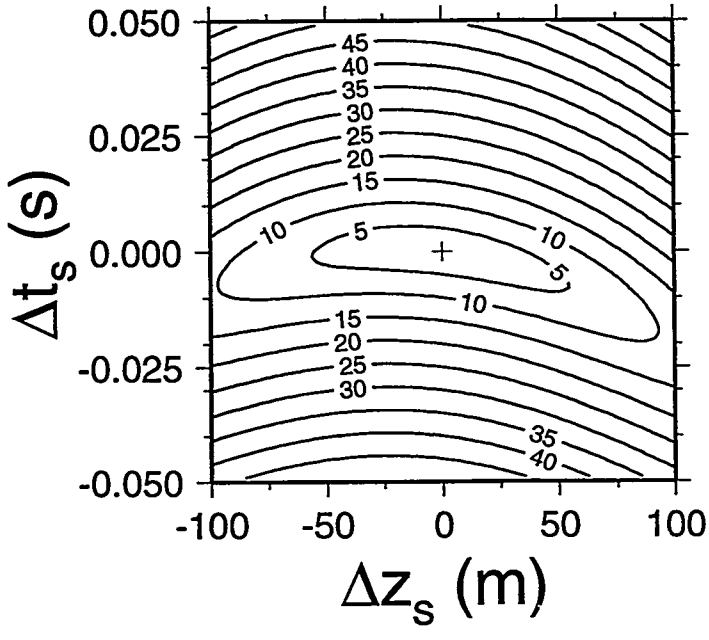
0.050
0.025
0.000
-0.025
-0.050
Δt_s (s)
-100
-50
0
50
100
Δz_s (m)
45
40
35
30
25
20
15
10
5
10
5
10
15
20
25
30
35
40

DISTRIBUTION LIST

Sandia National Laboratories Personnel

Organization 1612, Mailstop 1168:
H. Douglas Garbin

Organization 1707, Mailstop 1425:
Marion W. Scott

Organization 5736, Mailstop 0655:
Eric P. Chael
John P. Claassen

Organization 6116, Mailstop 0750:
David F. Aldridge (30 copies)
Sanford Ballard
Lewis C. Bartel
David J. Borns
Thurlow W.H. Caffey
Anthony DiGiovanni
Gregory J. Elbring
Bruce P. Engler
Joanne T. Fredrich
John C. Lorenz
Susan E. Minkoff
Gregory A. Newman
Neill P. Symons
Marianne C. Walck
Norman R. Warpinski
Chester J. Weiss
Christopher J. Young

Organization 6211, Mailstop 1033:
Douglas S. Drumheller

Organization 6533, Mailstop 1138:
Dorthe B. Carr

Organization 9124, Mailstop 0847:
Jeffrey L. Dohner

Organization 9221, Mailstop 1111:
Curtis C. Ober

Organization 9222, Mailstop 1110:
David E. Womble

Organization 15351, Mailstop 0859:
Mark D. Ladd
Gerard E. Sleefe
Terry K. Stalker

Technical Library: Organization 9616, Mailstop 0899 (2 copies)

Central Technical Files: Organization 8940-2, Mailstop 9018

Review and Approval Desk: Organization 9612, Mailstop 0612
For DOE/OSTI

Non-Sandia National Laboratories Personnel

Charles C. Burch
Conoco Incorporated
1000 South Pine
PO Box 1267
Ponca City, Oklahoma, 74602-1267

Andrew J. Calvert
Simon Fraser University
Department of Earth Sciences
8888 University Drive
Burnaby, British Columbia, Canada, V5A 1S6

Richard T. Coates
Schlumberger-Doll Research
Old Quarry Road
Ridgefield, Connecticut, 06877

Michael Fehler
Los Alamos National Laboratory
Mailstop D443
Los Alamos, New Mexico, 87545

Richard L. Gibson
Texas A&M University
Department of Geology and Geophysics
College Station, Texas, 77843-3115

Roland Gritto
Lawrence Berkeley National Laboratory
1 Cyclotron Road
Building 90, Mailstop 1116
Berkeley, California, 94720

Leigh House
Los Alamos National Laboratory
Earth and Environmental Sciences Division
Mailstop D-443
Los Alamos, New Mexico, 87545

Lane R. Johnson
University of California, Berkeley
Department of Geology and Geophysics
Berkeley, California, 94720

Robert T. Langan
Chevron Corporation
935 Gravier Street, Room 1661
New Orleans, Louiisiana, 70112

Ernest L. Majer
Lawrence Berkeley National Laboratory
1 Cyclotron Road
Building 90, Mailstop 1116
Berkeley, California, 94720

Keith L. McLaughlin
Science Applications International Corporation
1300 North 17th Street, Suite 1450
Arlington, Virginia, 22209

Mark A. Meadows
4th Wave Imaging
850 Glenneyre Street
Laguna Beach, California, 92651

James W. Rector, III
University of California, Berkeley
Department of Materials Science and Mechanical Engineering
557 Evans Hall
Berkeley, California, 94720

Gerard T. Schuster
University of Utah
Department of Geology and Geophysics
Salt Lake City, Utah, 84112

M. Nafi Toksoz
Massachusetts Institute of Technology
Earth Resources Laboratory
42 Carleton Street
Cambridge, Massachusetts, 02142